Numerical Analysis of the Shiaolin Landslide Using Material Point Method

Wei-Lin Lee[1], Mario Martinelli[2], and Chjeng-Lun Shieh[3]

[1]Department of Hydraulic and Ocean Engineering, National Cheng-Kung University, No.1, University Road, Tainan City 701, Taiwan (R.O.C.) Email: glaciallife@gmail.com
[2]Deltares, P.O. Box 177, 2600 MH Delft, The Netherlands. Email: Mario.Martinelli@deltares.nl
[3]Department of Hydraulic and Ocean Engineering, National Cheng-Kung University, No.1, University Road, Tainan City 701, Taiwan (R.O.C.) Email: shieh@dprc.ncku.edu.tw

Abstract: The Shiaolin landslide in southern Taiwan was triggered by Typhoon Morakot in 2009. The landslide carried out a volume that more than 22 million m^3 and travelled a distance that over 2 km. Many researchers conducted studies in the field investigations, laboratory experiments, and numerical simulation. However, the simulations of initial failure stage and post-failure stage had to implement separately due to the problem of mesh distortion. In this study, a fully dynamic and coupled two-phase formulations using material point method is used to simulate the entire landslide process. The topographies, field investigations, and laboratory experiments are used in the model. In the last section, the evolutions of sliding surface and the varying moving distances of landslide are discussed by the different thickness of infiltration zone and coefficients of friction along ground surface.

Keywords: Landslide; two-phase formulation; material point method; failure behavior.

1 Introduction

During heavy rainfall event related to Typhoon Marokot in august, 2009, a catastrophic landslide was triggered at Shiaolin village in Kaohsuing county, Taiwan. Kuo et al. (2013) estimated the magnitude of landslide based on the comparison of digital elevation model (DEM) before failure and after failure, as shown in Figure 1. The landslide carried out a volume over 22 million m^3 and moved over 2000 meter. Tsou et al. (2011) indicated that the velocity of landslide was over 20 m/s and the equivalent coefficient of friction was only about tan(14°). The avalanche caused the burial of Shiaolin village, the interruptions of bridges and roads, and over 400 fatalities. Because the catastrophic landslide was triggered by extreme rainfall event, many researchers were motivated to understand the occurrence and motion of this case study, and numerous field investigations, laboratory experiments, and numerical simulation were implemented in the past ten years (Lee et al. 2009; Tsou et al. 2011; Tsutsumi et al. 2011; Wu et al. 2013).

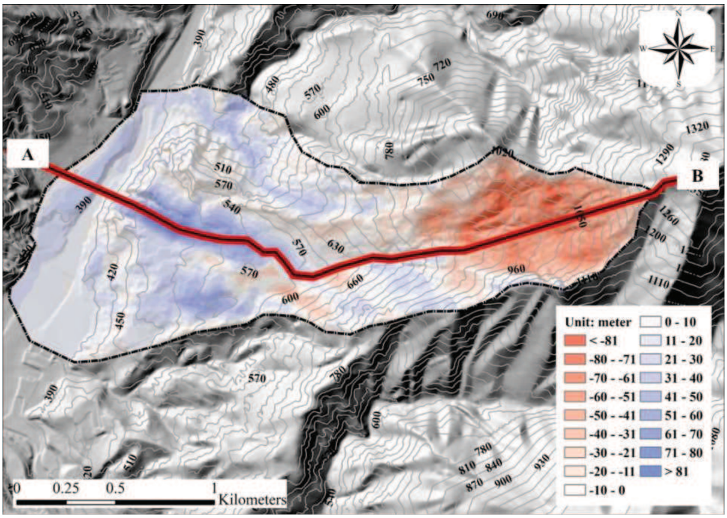

Figure 1. The comparison of the digital elevation model before and after Shiaolin landslide.

The past studies of the failure process can be divided in two groups: the first one looks at the onset of failure and the triggering conditions, the second one focuses on the post-failure analyses. The onset of failure can

Proceedings of the 7th International Symposium on Geotechnical Safety and Risk (ISGSR)
Editors: Jianye Ching, Dian-Qing Li and Jie Zhang

Published by Research Publishing, Singapore.
ISBN: 978-981-11-2725-0; doi:10.3850/978-981-11-2725-0_IS7-2-cd

be determined, for example, using finite element method or the limit equilibrium method (LEM) in combination with seepage flow analysis (Tsutsumi et al. 2011). Conversely, post-failure analyses are determined using large-deformation methods (i.e. rheological models, depth integrated models, and discontinuous deformation analysis) which are typically based on the assumption that the failure surface is provided before the calculation (Kuo et al. 2011; Kuo et al. 2013; Wu et al. 2013). The material point method (MPM) is one of the numerical approaches that can simulate both the onset and post-failure analysis during the same calculation.

MPM can be considered as an extension of the standard Finite Element Method, and it was introduced by Sulsky et al. (1994) to simulate large deformations process in single-phase materials. This approach avoids mesh distortion by combining the advantages of Lagrangian and Eulerian method, and it can simulate large deformation problems with history-dependent materials. Many researchers extended this method to simulate coupled hydro-mechanical problems in porous media (Zabala and Alonso 2011; Kafaji 2013; Jasmin et al., 2013, Abe et al. 2013). Some researchers also used MPM to investigate the entire failure process or rainfall induced landslides. In particular, Yerro et al. (2015) developed a full 3-phase formulation where the gas velocity is one of the primary unknowns of the system. Bandara et al. (2016) proposed a simplified version of 3-phase formulation, where suction and saturation are taken into account but the variation of gas pressure is assumed to be negligible. The latter formulation was implemented by Lee et al. (2019) to simulate the Fei Tsui Road landslide.

The problem of unsaturated infiltration was ignored in the present study because the investigations of soil water retention curve (SWRC) and relative permeability characteristic curve (RPCC) were fragmentary. In this paper, the failure process of Shiaolin landslide is simulated using the 2-phase formulation proposed by Jassim et al. (2013). In the failure stage, pore water pressure was an important factor in the triggering process, and the evolutions of sliding surface were discussed in the different thickness of infiltration zone. In the post-failure stage, the dynamic energy of landslide was dissipated due to friction on the ground surface, and so the varying moving distances of landslide were discussed in the different coefficients of friction on ground surface.

2 The Material Point Method

The set of equations of the dynamic formulation are described in this section, where the primary unknowns are the velocities of soil and water, indicated by the superscripts of *s* and *l* respectively ($\mathbf{v}^s$-$\mathbf{v}^l$ formulation) (Jassim et al. 2013).

The conservation of momentum of the mixture is written as follows

$$(1-n)\rho^s \boldsymbol{a}^s + n\rho^l \boldsymbol{a}^l = \nabla\cdot\boldsymbol{\sigma} + \rho^m \boldsymbol{b}\,, \tag{1}$$

where $\boldsymbol{b}$ is the body force vector, and $\boldsymbol{\sigma}$ is the total stress of the mixture, $\boldsymbol{a}^l$ and $\boldsymbol{a}^s$ are the acceleration of the liquid and soil phase, respectively. The density of the mixture ρ^m is determined as $\rho^m = \rho^s(1\text{-}n)+\rho^l n$, where n denotes the porosity, while ρ^l and ρ^s stand the constituent densities of the liquid and soil phase, respectively.

The generalized Darcy's law is introduced to describe dynamic of liquid phase in the porous media. The momentum balance of the liquid phase can be present by

$$\rho^l \boldsymbol{a}^l = \nabla p^l - \frac{n\mu^l}{k^l}\left(\boldsymbol{v}^l - \boldsymbol{v}^s\right) + \rho^l \mathbf{b}\,, \tag{2}$$

where μ^l is the dynamic viscosity of the liquid, p^l is the liquid pressure, and k^l is the intrinsic permeability of liquid, and $\boldsymbol{v}^l$ and $\boldsymbol{v}^s$ are the velocities of liquid and soli, respectively.

The conservation of mass of the solid phase is written as

$$\frac{\partial n}{\partial t} = (1-n)\nabla\cdot\boldsymbol{v}^s\,. \tag{3}$$

with the assumption that the solid particles are incompressible and the spatial gradient of the porosity is very small.

The liquid phase is considered as a weakly-compressible fluid, and the rate of liquid pore pressure is calculated as

$$\frac{\partial p^l}{\partial t} = \frac{K^l}{n}\left[(1-n)\nabla\cdot\boldsymbol{v}^s + n\nabla\cdot\boldsymbol{v}^l\right], \tag{4}$$

where K^l is the liquid bulk modulus. The stress-strain response of debris material is modelled as an elasto-plastic material with a failure criterion defined by Mohr-Coulomb.

A schematic representation of the material point method and the background mesh is shown in Figure 2. The points represent the material discretization and the background mesh is used for the computational step. Each material point carries information of the solid and liquid constituent, like mass, momentum, effective stress and liquid pressure. The background mesh is only used to solve the the $\boldsymbol{v}^s$-$\boldsymbol{v}^l$ formulation at the nodes and map information to particles. The explicit integration scheme, such as the one presented above, is conditionally stable. The size of the time step for stable solution depends on the properties of the materials: it decreases with stiffness and with low permeability.

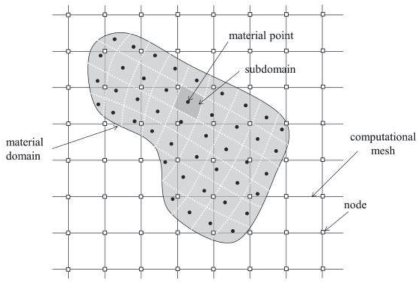

Figure 2. Spatial discretization in MPM (Yerro et al. 2015).

3 Geomorphology and Soil Properties of the Shiaolin Landslide

Figure 3 shows the region of source, transportation, and deposition of landslide along the cross section (AB) shown in Figure 1. According to the report of geological field survey (Lee et al. 2009), the slope in the source area is composed of a layer of Yenshuikeng shale (YS) overlay Tangenshan sandstone (TS). The failure surface was developed along the stratigraphic interface between YS and TS (Lee et al. 2009; Tsou et al. 2011).

To characterize the soil body of the landslide mass, soil samples of YS were taken from the source area. Wu et al. (2013) investigated the mechanical strength parameters of soil samples by several direct-shear tests according to the American standard test method (ASTM) D3080. According to the field survey report after the event (Lee et al. 2009), a significant part of landslide body was soaked due to the extreme rainfall event, and so the strength parameters were investigated in dry and saturated conditions. A clay fraction was found inside the soil body, which is classified as CL based on the United Soil Classification system. In high water content conditions, the clay fraction expands and becomes weaker, and so the strength parameter of YS decrease in saturated condition. The results of these experiments are summarized in Table 1. Wu et al. (2013) estimated Young's modulus and passion ratio of YS by ultrasonic test, which are 13.18 GPa and 0.20, respectively. The TS formation was recognized as an intact rock in the report of field investigation, and then it is assumed as an impermeable rigid body in the simulations. Wu et al. (2013) determined also the in-situ hydraulic conductivity tests by falling head tests after landslide occurred. The average hydraulic conductivity of the soils of TS is $1.48\text{x}10^{-6}$ m/s at the source area, with a range between $1.67\text{x}10^{-5}$ and $4.09\text{x}10^{-3}$ m/s at the region of transportation, and between $5.75\text{x}10^{-4}$ and $5.94\text{x}10^{-3}$ m/s at the deposition area. In this study, the conductivity of YS is set to 10^{-3} m/s constant during the simulation.

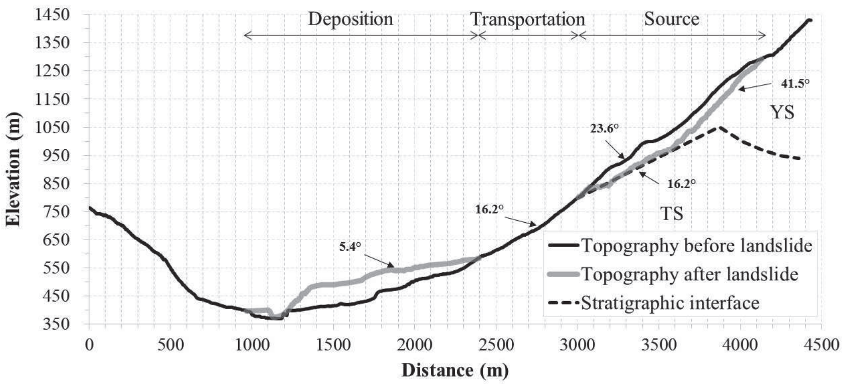

Figure 3. Profiles along cross section AB based on DTM data before and after landslide, YS is Yenshuikeng shale, TS is Tangenshan sandstone.

Table 1. Physical properties and strength parameters of YS

Physical properties	value	
Specific gravity	2.71	
	Dry condition	*Saturated condition*
Cohesion (MPa)	0.05 ~ 0.11	0 ~ 0.01
Friction angle (°)	37.2 ~ 45.1	21.4 ~ 25.5
Water content (%)	0.25 ~ 0.58	14.94 ~ 28.93

4 Numerical Model

Figure 4 shows the 2D plane strain numerical model, which was set up based on the cross section AB of Figure 3. The computational mesh has 48889 elements with 48888 material points. Three contact surfaces are defined in this study. The contact surface A, between TS and the dry part of YS, has a friction angle of 45° in agreement with the strength property of dried YS. A friction angle of 26° is assigned along the contact surface B. The frictional angle along contact surface C is varied between 10° and 20°, following the studies of Tsou et al. (2011).

The Shiaolin landslide was triggered by a severe rainfall event. However, in this study, the simulations do not consider the unsaturated flow due to unavailable data about the SWRC and RPCC. For this reason, the infiltration zone is set directly at the beginning of the calculation in the saturated domain (I), where the soil is assumed fully saturated with zero pore water pressure distribution. In the rest of domain, the soil is set to dry.

The thickness of the infiltration zone before the failure is unknown. Lee et al. (2009) reported a value of 80 m. In this paper, three values of infiltration depths are considered (20 m, 80m, and 200 m), estimated based on the duration of rainfall event (56 hr) and the conductivity range of YS. The strength parameters of the saturated and dry part correspond to the values in Table 1.

The numerical scheme is explicit, and the maximum time step is function of conductivity and bulk modulus the materials. In order to reduce the computational costs, the bulk modulus of liquid is decreased by a factor of 100.

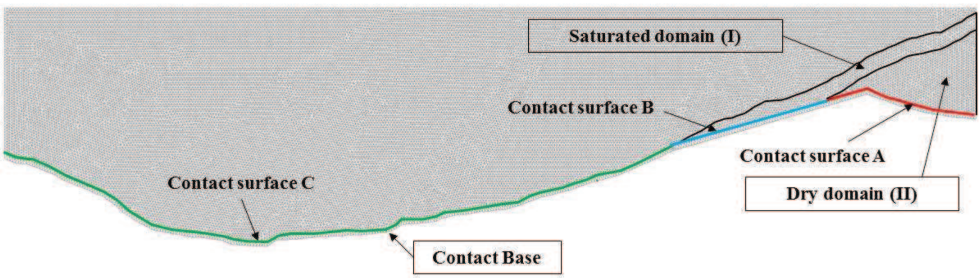

Figure 4. Summary of geometry and material domains for the Shiaolin landslide.

5 Numerical Results

The slope is stable in dry conditions, and it gets unstable at the toe due to water pressure build up. The magnitude and distribution of pore water pressure are strictly related to the initial thickness of the infiltration zone, which affect the position of the failure surface. Figure 5 (left) shows the size of the mobilized mass and the location of the failure surface for the three different thicknesses of the saturated zone. In all simulations the failure occurs in the saturated zone. For relatively shallow infiltration depth (20m), the failure zone is quite superficial without reaching the contact surface between YS and TS. In case of thick saturated zone (200m), the failure surface reaches the contact surface but it extends upstream involving a much larger volume compared to the field observations. The best agreement is observed for the thickness of 80m which is also in line with the conclusions of Lee et al. (2009).

The unstable material moves then from the source area to the deposition area. During the run-out process, the energy of the moving body is dissipated due to friction between soil and contact surface, and by the internal drag forces due to the presence of water into the soil body. The dissipation due to collision is not considered. Figure 5 (right) shows the final configuration of the moving mass in the deposition area for three different friction coefficients along the contact surface C. As expected, the lower the contact friction coefficient, the larger is the runout distance, with the best agreement when the contact friction angle is around 15°. This results is also in line with the conclusions of the report from Tsou et al. (2011), who proposed an equivalent friction angle for the Shiaolin landslide equal to 14°.

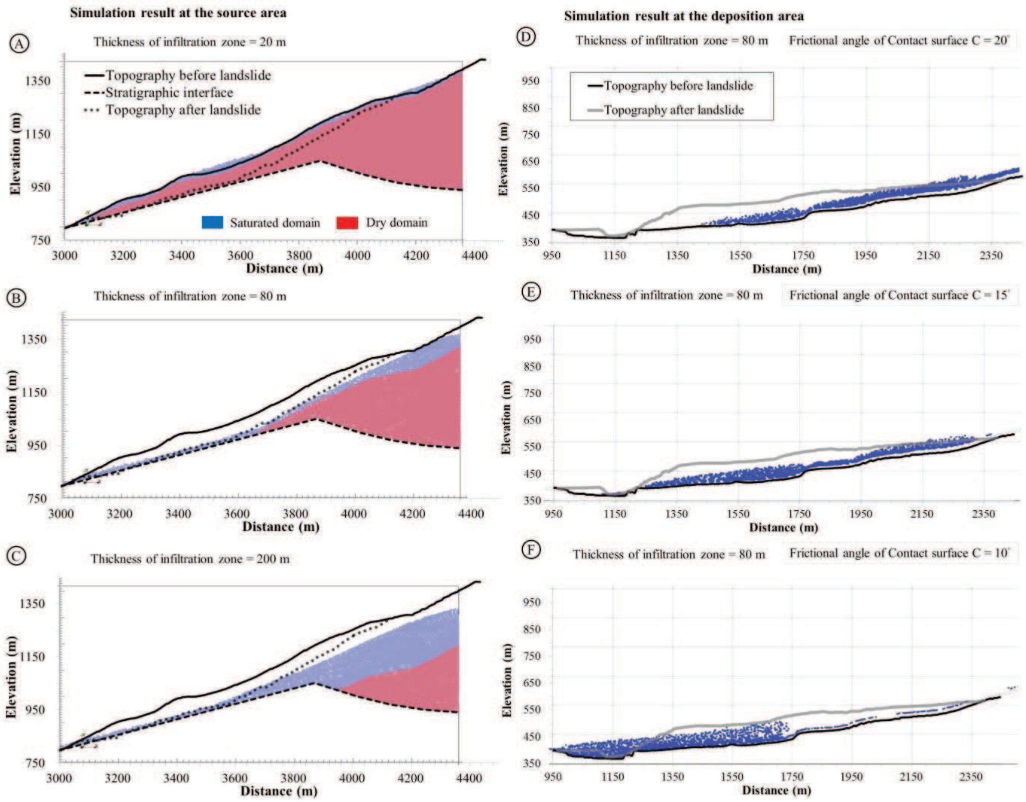

Figure 5. Simulation results at the source area (left side) and at the deposition area (right side).

錯誤! 找不到參照來源。 shows the failure process for the case with 80m of infiltration depth and friction angle equal to 15° along contact surface C. The beginning of landslide occurred at the toe of slope (Time = 15s) which moves downward. The sliding surface initially develops along the stratigraphic contact between YS and TS. During the process, larger mass located uphill is mobilized and moves downward (Time = 60s). At time t=120s, the front of moving material reaches the farthest location in the deposition area. Tsou et al. (2011) reported that the duration of major landslide was about 95s based on vibration signal of seismic stations and eyewitness reports. The duration of major landslide sounds a good agreement with field observations. After the major landslide occurred, the upper part of slope became unstable due to the removal of the toe. Then, the run out of residual material is continuing and the duration of entire landslide process is estimated over 5 min.

6 Conclusion

This paper presents a dynamic fully coupled formulation to simulate rainfall-induced landslides with the material point method. This numerical model is able to simulate both the onset of failure and the complete runout, avoiding the problem of mesh distortion, typical in the standard finite element method. With the MPM, a single analysis of the slope can be performed, without exchanging parameters from the stability analysis to post-failure analysis.

The Shiaolin landslide is simulated by the proposed model and the results of simulation is compared against field observations. Different thicknesses of infiltration zone and friction angles of contact surface are considered. Despite the fact that the failure process has a 3D component, the evolutions of sliding surface and moving distance computed with the 2D mode are in good agreement with previous studies and with field evidences.
The 3D effect will be evaluated in a following study, together with the use of a more advanced constitutive model which can take into account other sources of dissipation of energy (e.g., collisional).

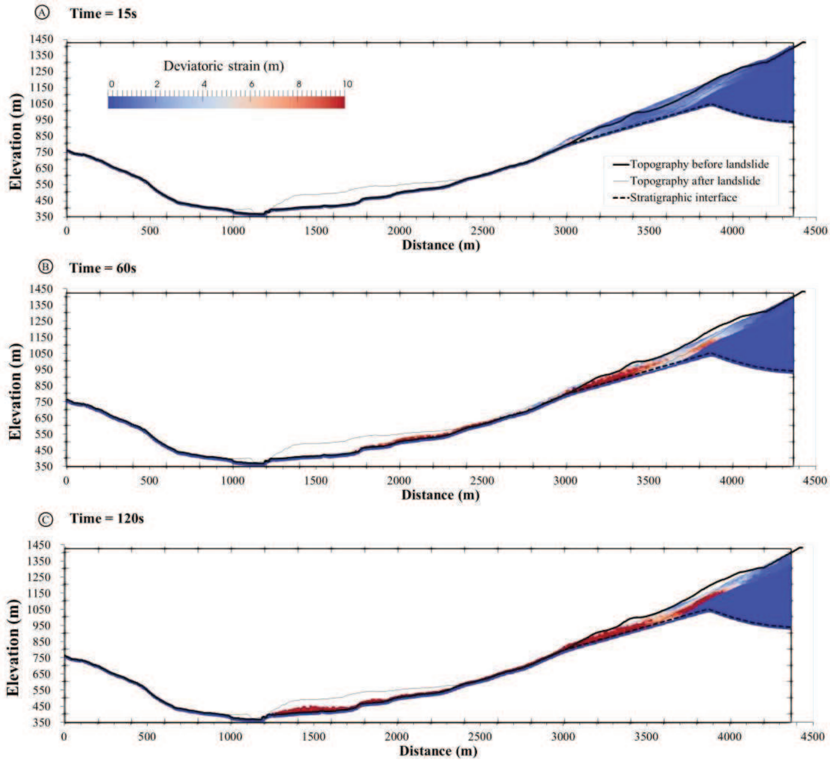

Figure 6. Landslide process of Shiaolin landslide; (A) time = 15s; (B) time = 60s; (C) time = 120s.

References

Abe, K., Soga, K., and Bandara, S. (2013). Material point method for coupled hydromechanical problems. *Journal of Geotechnical and Geoenvironmental Engineering*, 140(3), 04013033.

Bandara, S., Ferrari, A., and Laloui, L. (2016). Modelling landslides in unsaturated slopes subjected to rainfall infiltration using material point method. *International Journal for Numerical and Analytical Methods in Geomechanics*, 40(9), 1358-1380.

Jassim, I., Stolle, D., and Vermeer, P. (2013). Two-phase dynamic analysis by material point method. *International Journal for Numerical and Analytical Methods in Geomechanics*, 37(15), 2502-2522.

Kafaji, I.K.A. (2013). *Formulation of a Dynamic Material Point Method (MPM) for Geomechanical Problems*. PhD thesis, Universit¨at Stuttgart.

Kuo, C.Y., Tai, Y.C., Chen, C.C., Chang, K.J., Siau, A.Y., Dong, J.J., and Lee, C.T. (2011). The landslide stage of the Hsiaolin catastrophe: simulation and validation. *Journal of Geophysical Research: Earth Surface*, 116(F4).

Kuo, Y.S., Tsai, Y.J., Chen, Y.S., Shieh, C.L., Miyamoto, K., and Itoh, T. (2013). Movement of deep-seated rainfall-induced landslide at Hsiaolin Village during Typhoon Morakot. *Landslides*, 10(2), 191-202.

Lee, C.T., Dong, J.J., and Lin, M.L. (2009). Geological investigation on the catastrophic landslide in Siaolin Village, southern Taiwan. *Sino-Geotechnics*, 122, 87-94. (in Chinese)

Lee, W.L., Mario, M., and Shieh, C.L. (2019). Modelling rainfall-induced landslides with the material point method: the Fei Tsui Road case. *XVII European Conference on Soil Mechanics and Geotechnical Engineering*.

Sulsky, D., Chen, Z., and Schreyer, H.L. (1994). A particle method for history-dependent materials. *Computer Methods in Applied Mechanics and Engineering*, 118(1-2), 179-196.

Tsou, C.Y., Feng, Z.Y., and Chigira, M. (2011). Catastrophic landslide induced by typhoon Morakot, Shiaolin, Taiwan. *Geomorphology*, 127(3-4), 166-178.

Tsutsumi, D., Fujita, M., Miyamoto, K., Imaizumi, F., Fujimoto, M., Kokuryo, H., and Izumiyama, H. (2011). Analysis on the deep seated landslide occurred in Shaolin villege Kaohsiung county, Tiawan. *Journal of Japan Society of Civil Engineers*, Ser. B1 (Hydrau-lic Engineering), 67. (in Japanese)

Wu, J.H., Chen, J.H., and Lu, C.W. (2013). Investigation of the Hsien-du-Shan rock avalanche caused by typhoon Morakot in 2009 at Kaohsiung county, Taiwan. *International Journal of Rock Mechanics and Mining Sciences*, 60, 148-159.

Yerro Colom, A., Alonso Pérez de Agreda, E., and Pinyol Puigmartí, N.M. (2015). The material point method for unsaturated soils. *Géotechnique*, 65(3), 201-217.

Zabala, F., and Alonso, E.E. (2011). Progressive failure of Aznalcóllar dam using the material point method. *Géotechnique*, 61(9), 795-808.